RSC Advances

This article can be cited before page numbers have been issued, to do this please use: M. Chen, Z. Zhang, L. Li, Y. Liu, W. Wang and J. Gao, *RSC Adv.*, 2014, DOI: 10.1039/C4RA05186F.

View Article Online
DOI: 10.1039/C4RA05186F

Fast Synthesis of Ag-Pd@reduced graphene oxide bimetallic nanoparticles and their applications as carbon-carbon coupling catalysts

Mingxi Chen[a] Zhe Zhang[a] Lingzhi Li[a] Yu Liu[a*] Wei Wang[b] Jianping Gao[a*]

[a]School of Science, Tianjin University, Tianjin 300072, P R China

[b]School of Chemical Engineering, Tianjin University, Tianjin 300072, P R China

Abstract

Ultrafine Ag-Pd bimetallic nanoparticles homogeneously distributed on reduced graphene oxide (rGO) were prepared by redox reactions between Pd^{2+}, Ag^{+} and GO. This method is simple and the use of rGO as a support facilitated the separation and reuse of the Ag-Pd@rGO catalyst. The Ag-Pd@rGO bimetallic nanoparticles were characterized by ultraviolet-visible spectroscopy, Raman spectroscopy, thermogravimetric analysis, X-ray diffraction analysis, and X-ray photoelectron spectroscopy. The microstructure of the Ag-Pd@rGO was investigated with scanning electron microscopy and transmission electron microscopy. The Ag-Pd@rGO catalyst exhibited high catalytic activities in the Suzuki-Miyaura carbon coupling reaction and the Sonogashira carbon coupling (SCC) reaction. These reactions used mild, efficient, ligand-free and heterogeneous conditions. Interestingly, the presence or absence of oxygen in the SCC catalytic system resulted in two different products, which oxygen can be used as the control products "switch".

Keywords: alloys; composite materials; nanostructures

* Corresponding author. Tel.: +862227403475; Fax: (+86)22-2740-3475.
E-mail address: jianpinggaols@126.com (J.P. Gao).

View Article Online
DOI: 10.1039/C4RA05186F

1. Introduction

Noble metals with ultrafine sizes have attracted much interest because of their large surface areas and large numbers of edge and corner atoms, which greatly improves their catalytic activities and reduces the usage of the catalysts [1, 2]. However, nanoparticles usually suffer from aggregation which reduces their total surface energy [3]. In order to prevent aggregation, various stabilizers, such as surfactants and polymers, have been used to stabilize the nanoparticles [4]. Unfortunately, stabilizers can severely reduce the catalytic activity of the nanoparticles. Therefore, appropriate materials are needed to support nanoparticles in a manner that maintains their high catalytic activity.

Carbon materials, including carbon black, carbon nanotubes (CNTs), graphene and other derivatives have all been used as catalyst supports [5]. Among these carbon materials, graphene has recently attracted the most intense attention, due to its unique atom-thick 2D structure which has a high specific surface area, locally conjugated aromatic system, superior electron mobility, and high chemical and thermal stability [6, 7]. There have been many reports on the application of graphene as an ideal high performance support for metal, metal oxide and enzyme catalysts [7-9]. These studies have demonstrated that graphene can significantly enhance the catalytic activity of these catalysts [1, 10, 11].

Graphene oxide (GO) is a derivative of graphene which can be manufactured on a large scale at a relatively low cost by using natural graphite as the raw material. It contains oxygen-containing functional groups located mainly at the edges of the planes. This allows GO to easily disperse in water to form stable GO suspensions [12, 13]. Therefore, metal or metal oxides nanoparticles can be deposited onto the GO sheets. These graphene supported catalysts, including Au, Pt, FeO(OH), SnO_2, and TiO_2 are highly active photo-, electro- and chemical

View Article Online
DOI: 10.1039/C4RA05186F

catalysis [7,14-18].

Among the metallic catalysts, palladium-based catalysts have become a hot topic because of their outstanding performance in carbon−carbon cross-coupling [1, 19]. Three of the most important processes, the Heck reaction, Suzuki−Miyaura coupling, and the Sonogashira reaction have been widely studied with palladium catalysts in recent decades [20, 21]. However, commercial palladium-based catalysts are relatively expensive, and they are easily poisoned [22]. Moreover, they are sensitive to air and moisture, and require the addition of an organic ligand, such as triphenyl phosphine, which not only pollutes the environment, but also causes product separation issues. Heterogeneous catalysts can solve this problem [23]. For example, palladium-based catalysts can be fastened onto a solid phase carrier, so that the catalyst can be separated after the reaction and used repeatedly until it becomes inactivate. Recently, Jie et al. reported that Ag can play an auxiliary role in the catalytic cycle [24]. Therefore, bimetallic nanoparticles are expected to reduce the cost of catalysts and improve their resistance to poisoning.

Here, a facile and environmentally friendly method was established to prepare reduced graphene oxide (rGO) supported Ag-Pd@rGO bimetallic nanoparticles through a redox reaction between GO, Ag and Pd precursors. In this method, GO plays the role of both surfactant and support, and no additional surfactants were employed. The Ag-Pd@rGO bimetallic nanoparticles were characterized and their ability to catalyze carbon−carbon cross-coupling reactions was investigated using the Suzuki−Miyaura carbon coupling reaction, and the Sonogashira carbon coupling reaction. This is an efficient way to prepare Ag-Pd@rGO with excellent carbon−carbon coupling performance.

View Article Online
DOI: 10.1039/C4RA05186F

2. Experimental

2.1 Materials

Graphite was obtained from Huadong Graphite Factory. Palladium chloride, potassium tetrachloropalladate, copper sulfate, silver nitrate, chloroauric acid, chloroplatinic acid, iodobenzene, bromobenzene, phenylboronic acid, 1-bromo-4-nitrobenzene, 4-bromotoluene, 4-bromochlorobenzene, 4-bromoanisole, 4-bromoaniline, 1-bromo-4-iodobenzene and phenylacetylene were all purchased from Aladdin Industrial Co. Potassium permanganate, sodium nitrate, concentrated sulfuric acid, 30% hydrogen peroxide, sodium hydroxide, hydrochloric acid, potassium carbonate, triethylamine and azabenzene were all purchased from Tianjin Chemical Co. All chemicals were analytical grade and used as received.

2.2 Preparation of GO

GO was prepared from purified natural graphite by a modified Hummer's method [25]. Briefly, concentrated H_2SO_4 was added to a 250-mL flask filled with graphite, followed by the addition of $NaNO_3$, and then solid $KMnO_4$ was gradually added with stirring while the temperature was kept below 20 °C using a contact thermometer. Next the temperature was increased to 30 °C and excess distilled water was added to the mixture. Then the temperature was increased to 80 °C. Finally, 30% H_2O_2 was added until the color of mixture changed to brilliant yellow. The mixture was filtered and washed several times with 5% aqueous HCl to remove metal ions and then washed with distilled water to remove the acid. The resulting filter cake was dried in air then re-dispersed into water. Suspended GO sheets were obtained after ultrasonic treatment.

2.3 Synthesis of the Ag-Pd@rGO bimetallic nanoparticles

First, 5 mL of GO suspension (1 g/L), 5 mL of $AgNO_3$ (1.23×10^{-3} mol/L) and 5 mL of

View Article Online
DOI: 10.1039/C4RA05186F

$PdCl_2$ (1.23×10^{-3} mol/L) were mixed in a beaker. Next dilute sodium hydroxide solution (0.1 M) was added to adjust the pH to 8–9. Then the mixed solution was heated for 60 min at 85 °C with vigorous stirring. After its color changed from brown to black, the solution was centrifuged and washed several times with deionized water. Finally, the product was dried for 24 h at 60 °C in a vacuum oven to remove the water and then stored in a desiccator for further analysis.

2.4 Characterization of the Ag-Pd@rGO bimetallic nanoparticles

2.4.1 Ultraviolet-visible spectroscopy analysis

The UV-Vis absorption spectra of the GO and Ag-Pd@rGO suspensions were recorded with a TU-1901 UV-Vis spectrophotometer.

2.4.2 Transmission electron microscopy analysis

The sample for transmission electron microscopy (TEM) observation was prepared by placing drops of the diluted Ag-Pd@rGO aqueous suspension onto a carbon coated copper grid, which was then dried under ambient conditions prior to being introduced into the TEM chamber. TEM observation and energy dispersive X-ray spectroscopy (EDS) measurements were performed using a Philips Tecnai G2F20 microscope at 200 kV.

2.4.3 Raman microscopy analysis

Raman measurements were performed with an in Via Raman Microscope (RENISHAW, UK) high resolution Raman microscope, in a backscattered configuration.

2.4.4 X-ray diffraction analysis

The X-ray diffraction (XRD) diagrams of the samples were measured using an x-ray diffractometer (BDX3300) with reference target: Cu Ka radiation (λ = 1.54 Å), voltage: 30 kV and current: 30 mA. The samples were measured from 10º to 40º (2θ) with steps of 4 º min^{-1}.

View Article Online
DOI: 10.1039/C4RA05186F

2.4.5 Thermogravimetric analysis

The samples were first dried in a vacuum at 40 °C for 2 days before the thermogravimetric analysis (TGA) was recorded with a Rigaku-TD-TDA analyzer with a heating rate of 10 °C/min.

2.4.6 X-ray photoelectron spectroscopy (XPS) analysis

Elemental analysis of the Ag-Pd@rGO was conducted on an x-ray photoelectron spectrometer with an Mg Kα anode (PHI1600 ESCA System, PERKIN ELMER, US).

2.5 Chemical reaction catalyzed by Ag-Pd@rGO bimetallic nanoparticles

2.5.1 General procedure for the Suzuki−Miyaura carbon coupling (SMCC) reaction

Phenylboronic acid (0.5 mmol, 1 equiv), aryl bromide (0.6 mmol, 1.2 equiv), potassium carbonate (1.0 mmol, 2 equiv) and Ag-Pd@rGO (1 mg, Pd 0.3% (atomic %), ~0.0003 equiv) were added to a 25-mL Schlenk flask that was then sealed with a Teflon screw cap. The flask was connected to the Schlenk line and evacuated by a vacuum. The flask was then flushed with nitrogen before nitrogen-purged water (2.0 mL) was added via a syringe. The flask was transferred to a preheated oil bath at 80 °C and the mixture was allowed to react for 10 h with stirring. After cooling to room temperature, the product was extracted into ethyl acetate, dried over Na_2SO_4 and then analyzed by Gas Chromatography-Mass Spectrometry (GC-MS). Finally, the product was purified via flash chromatography (silica gel) using 10% ethyl acetate in petroleum ether as the eluent and the product was analyzed by ^{1}H nuclear magnetic resonance (^{1}HNMR).

2.5.2 Gas Chromatography-Mass Spectrometry

A Gas Chromatograph (TRACEDSQ, Thermo Finnigan, US), equipped with a capillary column (30 m, 0.25 mm i.d., 0.25 μm film thickness) and a mass spectrometer (TRACEDSQ,

View Article Online
DOI: 10.1039/C4RA05186F

Thermo Finnigan, US), was used to analyze the products. The carrier gas was nitrogen, at a flow rate of 1 mL/min. The column temperature was initially 100 °C for 2 min, then gradually increased to 250 °C at 20 °C/min, and finally maintained at 250 °C for 2 min. For GC-MS detection, an electron ionization system with an ionization energy of 70 eV was used. The extracts were diluted 1:100 (v/v) with ethyl acetate, and 1.0 μL of the diluted samples was manually injected in the splitless mode.

2.5.3 General procedure for the Sonogashira carbon coupling (SCC) reaction

Phenylacetylene (0.5 mmol, 1 equiv), iodobenzene (0.6 mmol, 1.2 equiv), potassium carbonate (1.0 mmol, 2 equiv) and Ag-Pd@rGO (1 mg, Pd 0.3% (atomic %), ~0.0003 equiv) were added to a 25-mL Schlenk flask that was then sealed with a Teflon screw cap. The flask was connected to the Schlenk line and evacuated by a vacuum. The flask was then flushed with nitrogen before nitrogen-purged water (2.0 mL) was added via a syringe. Then, the flask was transferred to a preheated oil bath at 85 °C and allowed to react for 10 h with stirring. After cooling to room temperature, the product was extracted into ethyl acetate, dried over Na_2SO_4 and subjected to GC-MS analysis. The product was purified via flash chromatography (silica gel) using 10% ethyl acetate in petroleum ether as the eluent.

3. Results and Discussion

3.1 The transformation of GO during the reaction

The Ag-Pd@rGO bimetallic nanoparticles were prepared by direct reactions between the GO and the metallic precursors. In order to explore the transformation of GO during the reaction, the products were characterized with UV-Vis, Raman spectroscopy, TGA, XRD and XPS. Ultraviolet-visible spectroscopy is a useful tool to characterize the structural changes of

View Article Online
DOI: 10.1039/C4RA05186F

graphene oxide before and after reactions. As shown in Fig. 1a, the maximum absorption peak (λ_{max}) of the GO suspension is at 232.6 nm, but after the reaction, the peak red-shifted to 268.4 nm. This demonstrates that the GO was reduced and the electronic conjugation within the graphene nanosheets was restored during the reaction [26]. Since GO can be reduced in NaOH solution, a control experiment was also conducted. GO was added to a solution of NaOH and heated in the same conditions for 60 min at 85 °C. Under these conditions, the maximum absorption peak red shifted, but only to 251.3 nm. Therefore, the reduction of GO in Ag-Pd@rGO may be attributed to a cooperative action between the NaOH and the metallic precursors.

Raman spectroscopy is also widely used to analyze carbon materials and can provide information about defect density and structures, disorder and doping levels [27]. Generally, the Raman spectrum of graphene is characterized by two main features, the G mode arising from the first order scattering of the E_{2g} phonons of sp^2 C atoms (usually observed at ~1575 cm^{-1}) and the D mode due to the breathing mode of κ-point phonons with A_{1g} symmetry (at ~1350 cm^{-1}). Changes in the relative intensities of the D and G bands (D/G) indicate changes in the electronic conjugation state of the GO. The Raman spectra of GO and Ag-Pd@rGO are shown in Fig. 1b. The D/G ratio of GO increased from 0.99 to 1.21 after the reaction. This increase suggests that sp^2 domains were formed during the reaction and GO was reduced [28].

Figure 1c shows the XRD patterns of pristine graphite, GO and RGO. Graphite has a narrow and strong diffraction peak at around 2θ = 26.5° (d-spacing is 0.34 nm), but GO has a broad peak at about 11.4° (the interlayer spacing is 0.78 nm). This peak is due to the oxygen-containing functional groups. The larger interlayer distance can be attributed to the formation of hydroxyl, epoxy, and carboxyl groups which increases the distance between the

View Article Online
DOI: 10.1039/C4RA05186F

layers. After the reaction, this peak disappeared and there is a decrease in the interlayer spacing which indicates that the oxygen-containing functional groups have been removed. These results are consistent with the results for rGO reduced chemically (with $NaBH_4$) or thermally and thus indicate that GO was reduced here [29].

The reduction of GO was also confirmed by TGA and the results are shown in Fig. 1d. The GO has two main weight losses. The first rapid weight loss (~15%) from 30 to 150 ºC is due to the dehydration of the GO. The second weight loss (~25%) between 200 and 250 ºC represents the decomposition of the oxygen-containing functional groups [27]. In Ag-Pd@rGO, the second weight loss is obviously much lower than that in GO, indicating that most of the oxygen-containing functional groups were removed during the reaction.

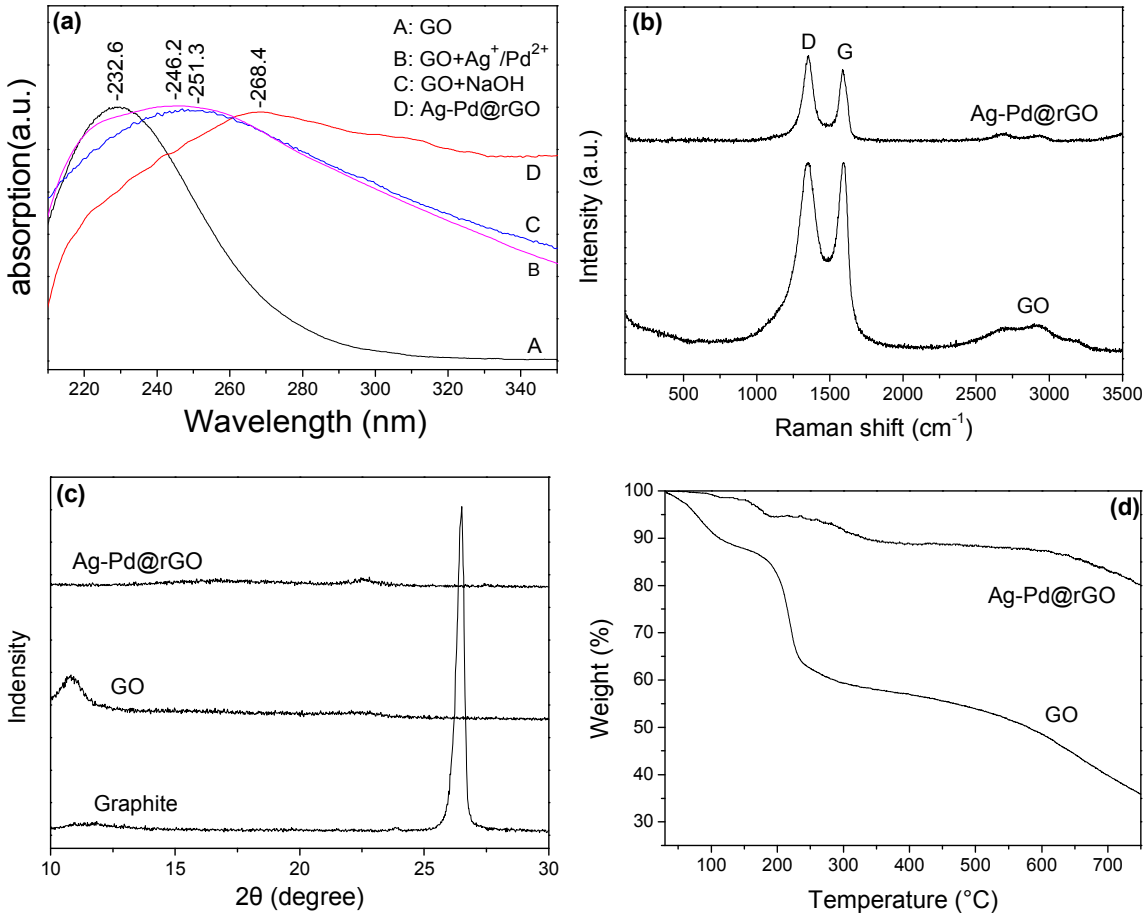

Figure 1. (a) UV-Vis absorption spectra of the GO, GO+Ag^+/Pd^{2+}, GO+NaOH and

View Article Online
DOI: 10.1039/C4RA05186F

Ag-Pd@rGO; (b) Raman spectra of GO and Ag-Pd@rGO; (c) XRD patterns of graphite, GO and Ag-Pd@rGO; and (d) TGA curves of GO and Ag-Pd@rGO

In addition to the above qualitative analyses, a quantitative analysis of the GO and Ag-Pd@rGO was carried out by XPS and the results are shown in Fig. 2 and Table 1. The relative oxygen content of the Ag-Pd@rGO bimetallic nanoparticles is obviously lower than that of pristine GO (Fig. 2a) and the elemental ratio of C/O increased from 2.9 to 6.1 (Table 1), which is higher than that in rGO reduced by $NaBH_4$ (4.78) [30].

The C_{1s} peaks for GO and the Ag-Pd@rGO bimetallic nanoparticles are shown in Figs. 2b and 2c. The spectrum of C_{1s} can be deconvoluted into three peaks at 284.5, 286.4, and 288.0 eV which are attributed to C=C double bonds, C-O single bonds of the epoxy and/or the alkoxy groups, and C=O double bonds, respectively [27]. After the reaction, the relative intensity of the peaks at 286.4 eV and 288.0 eV decreased whereas the relative intensity of the peak at 284.5 eV increased significantly. These changes clearly demonstrate the removal of the oxygen-containing groups and the formation of sp^2 domains in GO. The XPS results further prove that GO was reduced. In addition to the C and O peaks, the XPS spectrum of Ag-Pd@rGO also shows Ag and Pd peaks. This indicates that rGO contained Ag and Pd (Figs. 2d and 2e) which will be discussed in the next section.

View Article Online
DOI: 10.1039/C4RA05186F

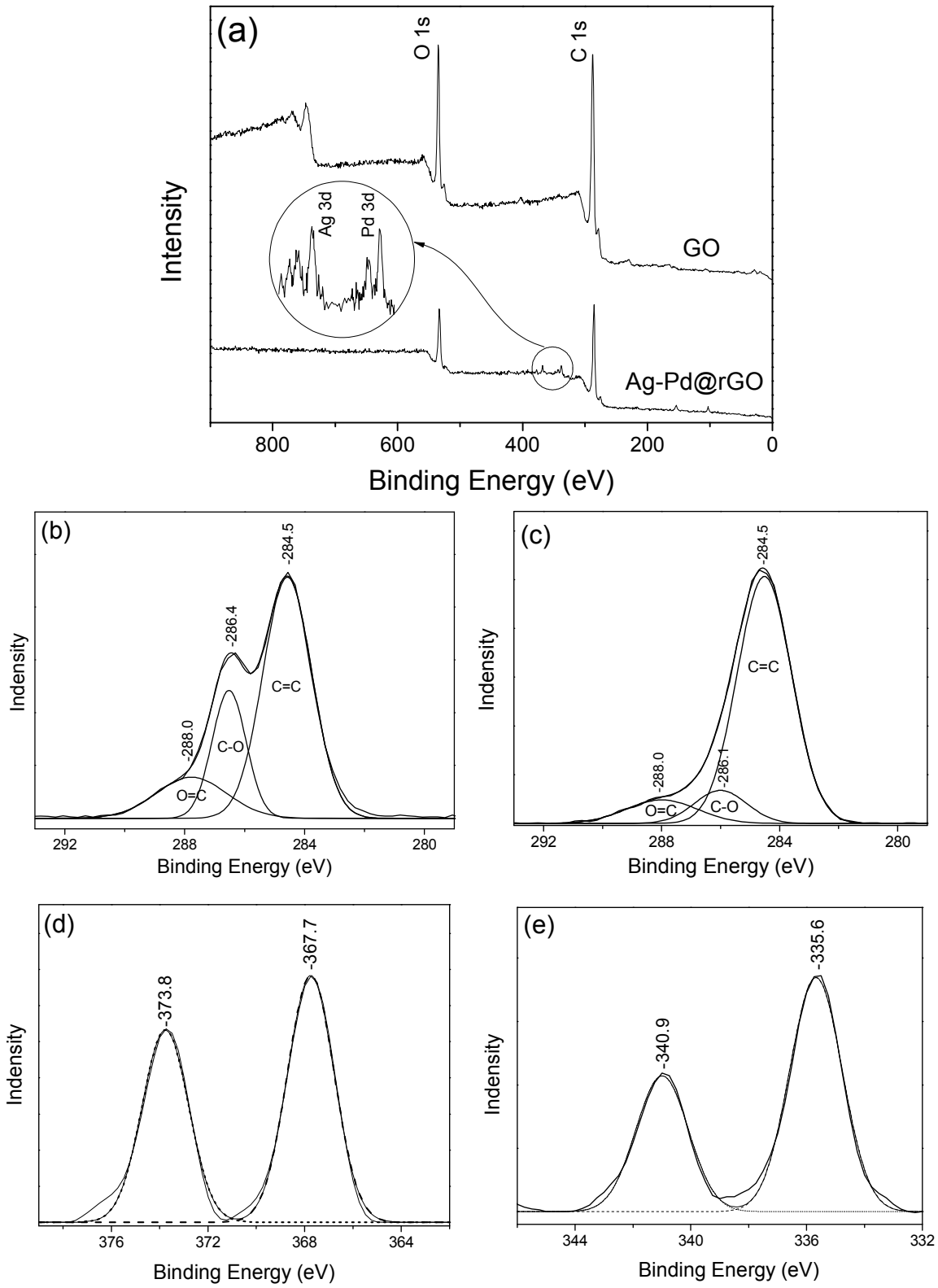

Figure 2. (a) XPS spectra of GO and Ag-Pd@rGO, the inset is the magnified spectra of the Ag_{3d} peaks and Pd_{3d} peaks of Ag-Pd@rGO; (b) curve fit for C_{1s} of GO; (c) curve fit for C_{1s} of Ag-Pd@rGO; (d) curve fit for Ag_{3d} of Ag-Pd@rGO; and (e) curve fit for Pd_{3d} of Ag-Pd@rGO.

View Article Online
DOI: 10.1039/C4RA05186F

Table 1. Percentage of carbon, oxygen, palladium and silver in GO and Ag-Pd@rGO

Sample	Analysis				
	Carbon	**Oxygen**	**Silver**	**Palladium**	**C/O ratio**
GO	75.2	24.8	0	0	2.9
	C=C	**C-O**	**C=O**		
	61.9	22.9	15.2		
	Carbon	**Oxygen**	**Silver**	**Palladium**	**C/O ratio**
Ag-Pd@rGO	85.4	13.9	0.3	0.3	6.1
	C=C	**C-O**	**C=O**		
	80.0	10.0	9.9		

3.2 The transformation of the metal ions during the reaction

XPS can not only characterize the transformation of GO during the reaction, but also those of $AgNO_3$ and $PdCl_2$. The Ag_{3d} spectrum of Ag-Pd@rGO (Fig. 2d) has two peaks. The one at 367.7 eV is attributed to $Ag_{3d5/2}$ and the other at 373.8 eV is due to $Ag_{3d3/2}$. Similarly, the Pd_{3d} spectrum also has two peaks (Fig. 2e); the peaks at 335.6 and 340.9 eV correspond to $Pd_{3d5/2}$ and $Pd_{3d3/2}$ respectively. These results indicate that the Ag^+ and Pd^{2+} ions were transformed to Pd^0 and Ag^0 and attached to the rGO nanosheets.

The Pd^0 and Ag^0 were produced through redox reactions between the GO and the metallic precursors. It is speculated that the standard electrode potential is the key factor in determining the redox reaction. Table 2 shows the standard electrode potentials of Au(Ⅲ), Pt(Ⅱ), Ag(Ⅰ), Pd(Ⅱ) and Cu(Ⅱ) under alkaline condition. The electrode potential of GO is +0.48 (relative to the standard hydrogen electrode).[1] Therefore, when the standard electrode potential of an ion is

View Article Online
DOI: 10.1039/C4RA05186F

greater than +0.48, it can be reduced by GO. The standard electrode potentials of Ag^+ and Pd^{2+} are both lower than that of GO; however, adjusting the pH and concentration of the precursors changes the potential of Ag^+ and Pd^{2+} so they can be reduced.

In order to confirm this conjecture, five different salt solutions (shown in Table 2) were reacted with GO under identical conditions, and the products were characterized by XRD (Fig. 3). In the XRD pattern of Ag/rGO, the peaks at 38.1°, 44.3°, 64.4° and 77.4°, correspond to the face-centered cubic (fcc) structure of Ag (111), (200), (220) and (311), respectively (Joint Committee on Powder Diffraction Standards (ICSD, 87-0597). Similarly, the other four spectra confirm the existence of Au (ICSD, 04-0784), CuO (ICSD, 80-1916), Pt (ICSD, 01-1190), and Pd (ICSD, 46-1043), which coincides with the products predicted in Table 2. These results support the conjecture that Pd^0 and Ag^0 were produced through redox reaction between the GO and the metallic precursors.

Table 2. Standard electrode potentials of some ions at 298K

Reactants	Products	Electrode Reaction	Standard Electrode Potential (E^θ (V))
$HAuCl_4$	Au	$[AuCl_4]^- + 3e^- = Au + 4Cl^-$	+1.002
K_2PtCl_4	Pt	$[PtCl_4]^{2-} + 2e^- = Pt + 4Cl^-$	+0.755
$AgNO_3$	Ag	$Ag_2O + H_2O + 2e^- = 2Ag + 2OH^-$	+0.342
$PdCl_2$	Pd	$Pd(OH)_2 + 2e^- = Pd + 2OH^-$	+0.07
$CuSO_4$	CuO	$Cu(OH)_2 + 2e^- = Cu + 2OH^-$	-0.222

View Article Online
DOI: 10.1039/C4RA05186F

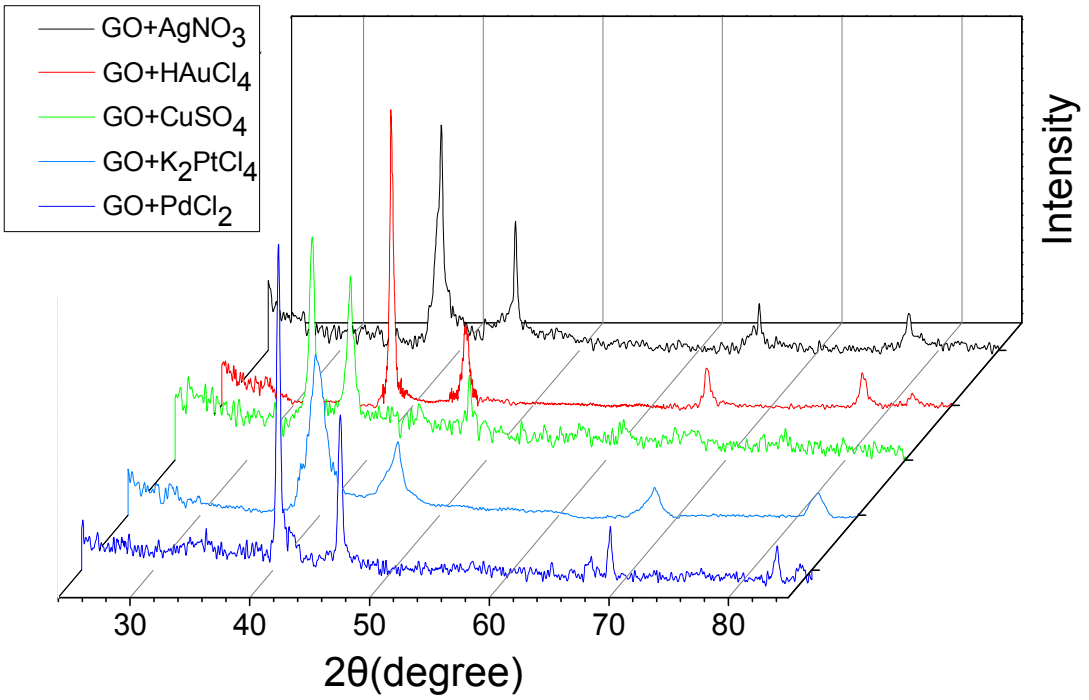

Figure 3. XRD patterns of Ag/rGO, Au/rGO, CuO/rGO, Pt/rGO and Pd/rGO

The TEM photos in Fig. 4 give a more direct view of the morphology of the Ag-Pd@rGO. The Ag-Pd@rGO was dispersed in ethanol, transferred to a 200-mesh, carbon-coated copper grid and then observed by TEM. Nanoparticles with diameters of ~10 nm are uniformly distributed on the GO nanosheets (Fig. 4a). In the high magnification view (Fig. 4b), different lattice fringe structures are observed on the surfaces of most of the nanoparticles which indicates that each nanoparticle contains different crystal structures.

Figure 4c is the EDX spectrum of a single nanoparticle, and it clearly shows that the nanoparticle is composed of Pd and Ag. Other particles were also analyzed by EDX and the results were similar. Figure 4d shows the cross-sectional compositional line profiles measured over the nanoparticle. Both the Ag and Pd elements appear to be quite evenly distributed along the line. This is clear evidence that Ag-Pd bimetallic nanoparticles are loaded onto the rGO.

View Article Online
DOI: 10.1039/C4RA05186F

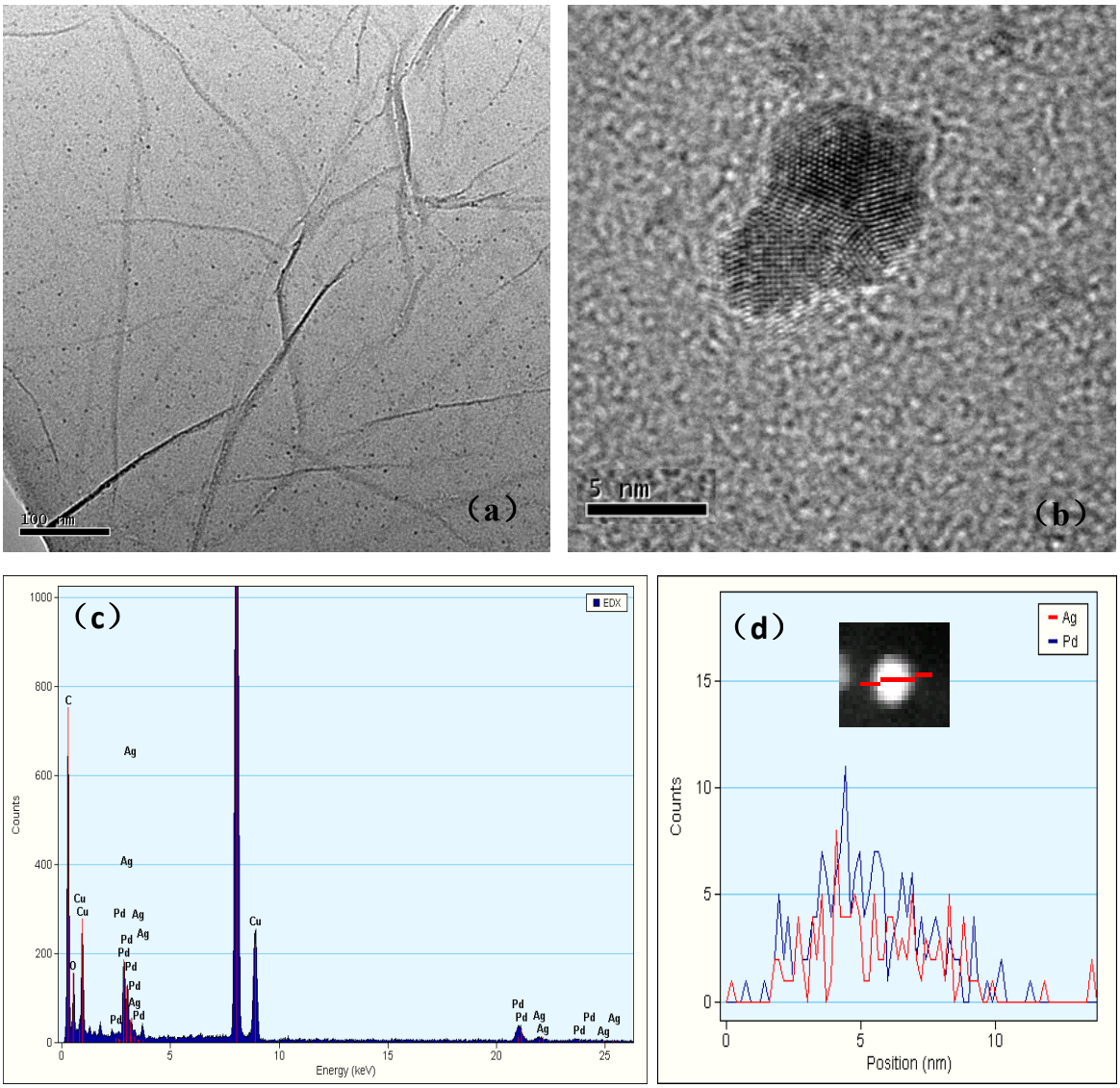

Figure 4. TEM images of the Ag-Pd@rGO with the scale of (a) 100 nm and (b) 5 nm; (c) EDX of Ag-Pd@rGO; and (d) Cross-sectional compositional line profiles for Ag-Pd@rGO

UV-Vis analysis was also conducted and the spectra are shown in Fig. 5. The UV-Vis spectrum of Ag/rGO has a peak at 410 nm which is due to the absorption of the Ag nanoparticles. The Pd/rGO spectrum does not have a peak at this wavelength and the Ag-Pd@rGO spectrum has a relatively weak peak. This confirms the existence of Ag-Pd bimetallic nanoparticles.

View Article Online
DOI: 10.1039/C4RA05186F

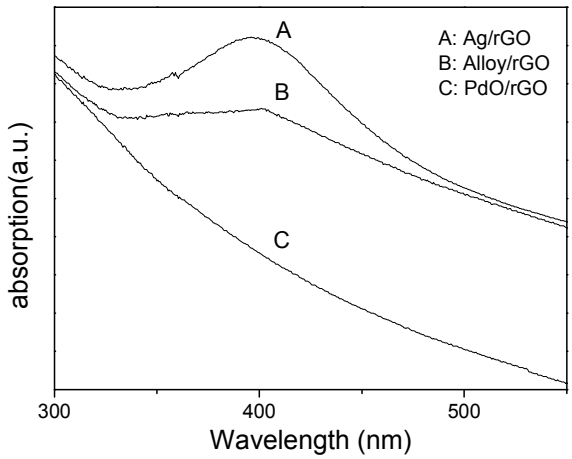

Figure 5. UV-Vis absorption spectra of the Ag/rGO, Ag-Pd@rGO and Pd/rGO

3.3 Catalytic activity of Ag-Pd@rGO in Sonogashira carbon coupling (SCC) reaction

The catalytic activity of Ag-Pd@rGO in the Sonogashira reaction was also explored and the results are shown in Table 3 and Fig. S1. The expected product is the cross-coupling product, 1,2-diphenylethyne (**2a**), but interestingly, 1,4-diphenylbuta-1,3-diyne (**2b**) which is a homocoupling by-product, was dominant under some conditions [31]. The reaction was performed with different alkali salts and in different gas environments to investigate their effects on the reaction.

The Ag catalyst was inactive under a nitrogen atmosphere. However, the activity of the Ag-Pd@rGO catalyst was relatively high in the SCC reaction with a yield of 92% of **2a** which was a little higher than that for the Pd catalyst (86%). The solvent and the reactants were sparged with nitrogen gas before the reaction to remove any dissolved oxygen and the reaction was carried out in a Schlenk tube which prevented the introduction of any oxygen into the reaction system. With no oxygen present, the products contain almost no **2b**. (Table 3: entries 1-3)

When the gas environment was changed, the yields of **2a** and **2b** also changed. For the

View Article Online
DOI: 10.1039/C4RA05186F

reaction under air, the yield of **2a** was much less and the yield of **2b** increased. When oxygen was introduced during the reaction, the product contained only **2b**. Therefore, the atmosphere controls which type of reaction occurs, cross-coupling or homocoupling. By adjusting the oxygen content, the ratio of **2a** to **2b** can be adjusted. (Table 3: entries 3, 7, 9)

The catalytic efficacy was further evaluated by adding different alkali salts. The yield dropped significantly in the presence of a strong base like NaOH. The catalytic activity of Ag-Pd@rGO in the presence of triethylamine was better than that with NaOH (Table 3: entries 4, 5). However the addition of triethylamine, causes the Ag-Pd@rGO catalyst to cross-link, which can create difficulties in separating and recycling the catalyst. Therefore, K_2CO_3 is the most effective alkali in terms of activity, selectivity and recyclability (Table 3: entries 3-9).

Table 3. Sonogashira carbon coupling reaction of iodobenzene and phenylacetylene

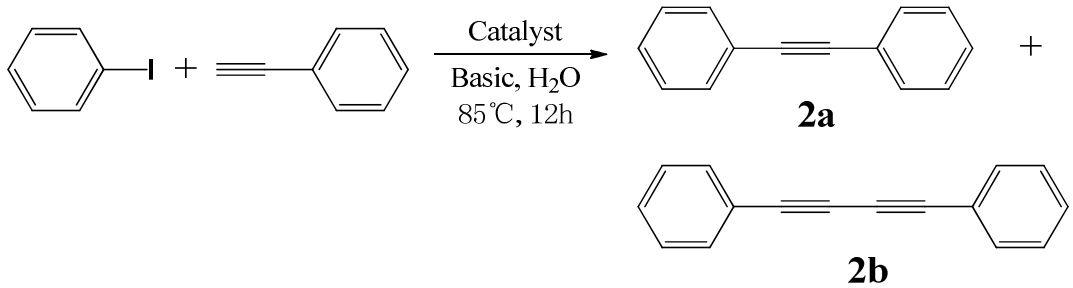

Entry	Atmosphere	Alkali	Catalyst	Yield of **2a**	Yield of **2b**
1	N_2	K_2CO_3	Ag	Trace	Trace
2	N_2	K_2CO_3	Pd	86%	Trace
3	N_2	K_2CO_3	Ag-Pd@rGO	92%	Trace
4	N_2	Et_3N	Ag-Pd@rGO	81%	Trace
5	N_2	NaOH	Ag-Pd@rGO	74%	Trace
6	Air	NaOH	Ag-Pd@rGO	12%	Trace
7	Air	K_2CO_3	Ag-Pd@rGO	7%	72%

View Article Online
DOI: 10.1039/C4RA05186F

8	Air	Et_3N	Ag-Pd@rGO	Trace	34%
9	O_2	K_2CO_3	Ag-Pd@rGO	Trace	85%

3.4 Catalytic activity of Ag-Pd@rGO in Suzuki−Miyaura carbon coupling (SMCC) reaction

The SMCC reaction was selected as a model reaction to investigate the catalytic activity of Ag-Pd@rGO. The SMCC reaction is most efficient under basic conditions and it has been reported that the presence of K_2CO_3 makes the reaction more efficient [32]. Kim et. al have reported that rGO can be used as a phase transfer agent, and that it tends to be present between the organic and aqueous phases [33]. The catalytic activity of Ag, Pd and Ag-Pd@rGO were tested for the SMCC reaction of 4-methylphenylboronic acid and different bromobenzenes under heterogeneous conditions with K_2CO_3 as an acid binding agent. The results are shown in Table 4 and according to the GC results (Fig. S2-S9) the product was pure.

The catalytic activity of Ag was very low in the SMCC reaction and the catalytic ability of Ag-Pd@rGO was similar to that of Pd. If the functional group on the p-arylbromide was a strong electron withdrawing group, the yield of the SMCC reaction was very high (> than 99%) due to electronic effects; however, if the functional group was an electron donor group, the yield of the SMCC reaction was slightly lower.

Since the nitro-group is an electron withdrawing group and the yield of this reaction was >99% for both Pd and Ag-Pd@rGO, the reaction between phenylboronic acid and 1-bromo-4-nitrobenzene was selected to explore the reusability of the catalysts. The results are shown in Fig. 6. The Pd catalyst quickly lost its activity upon reuse which demonstrates the poisoning of catalyst. However, the Ag-Pd@rGO catalyst could be recycled 10 times with a

View Article Online
DOI: 10.1039/C4RA05186F

negligible drop in activity and achieved a total turnover number of more than 30,000. Meanwhile, after catalytic reaction, the morphology of the catalyst did not change much (Fig. S10). The good recyclability of Ag-Pd@rGO provides a way to greatly reduce the cost of the catalyst.

Table 4. Suzuki−Miyaura carbon coupling reaction of phenylboronic acid and arylbromide

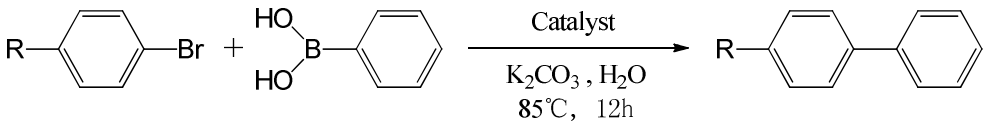

Entry	Arylbromide	Product	Catalyst	Yield*	TON*
1	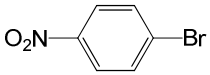	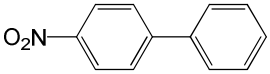 1a	Ag	Trace	----
2			Ag-Pd@rGO	>99%	3333
3			Pd	>99%	2000
4	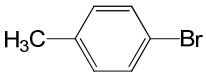	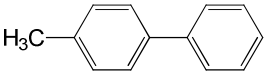 1b	Ag	Trace	----
5			Ag-Pd@rGO	90%	3000
6			Pd	89%	1780
7	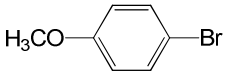	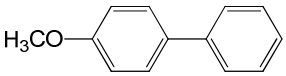 1c	Ag	Trace	----
8			Ag-Pd@rGO	98%	3267
9			Pd	98%	1960
10	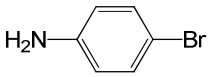	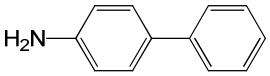 1d	Ag	Trace	----
11			Ag-Pd@rGO	91%	3033
12			Pd	92%	1840
13	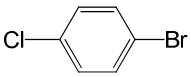	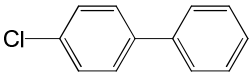 1f	Ag	Trace	----
14			Ag-Pd@rGO	>99%	3333
15			Pd	92%	1840

View Article Online
DOI: 10.1039/C4RA05186F

16	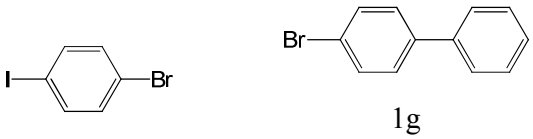	1g	Ag	Trace	----
17			Ag-Pd@rGO	>99%	3333
18			Pd	>99%	2000
19	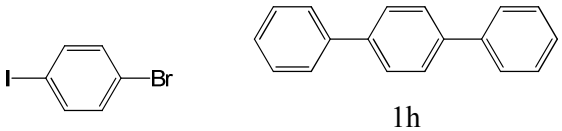	1h	Ag	Trace	----
20			Ag-Pd@rGO	>99%	3333
21			Pd	97%	1940
22	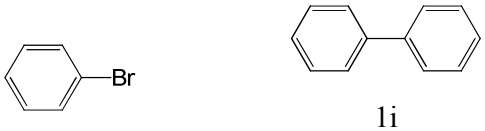	1i	Ag	Trace	----
23			Ag-Pd@rGO	>99%	3333
24			Pd	>99%	2000

*TON is defined as mole substrate reacted per mole catalyst
*Yield was determined by GC and TON was calculated from GC yield.

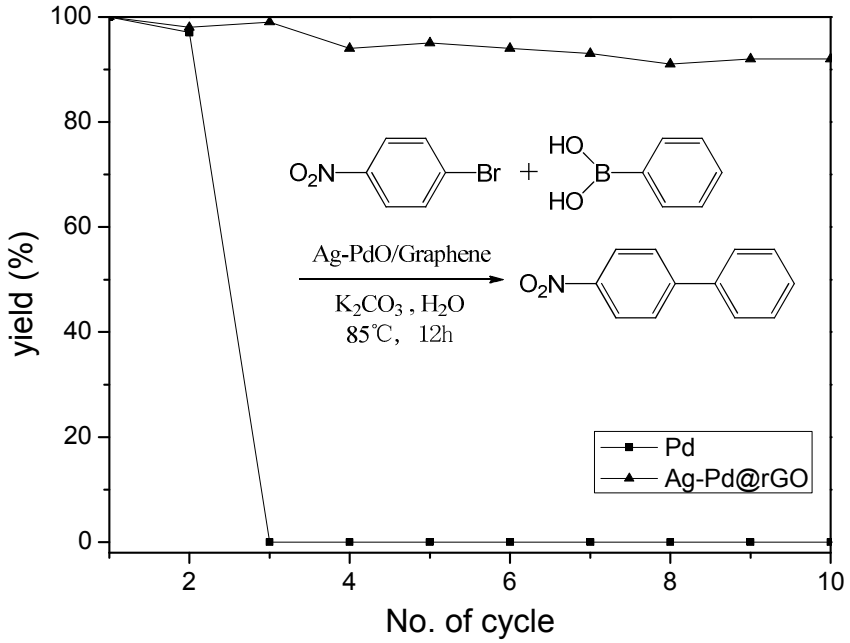

Figure 6. Recyclability of the Ag-Pd@rGO catalyst in the reaction of phenylboronic acid and 1-bromo-4-nitrobenzene

View Article Online
DOI: 10.1039/C4RA05186F

4. Conclusions

In summary, a facile method for synthesizing Ag-Pd@rGO bimetallic nanoparticles with a homogeneous distribution using a redox reaction between Pd^{2+}, Ag^{+} and and GO has been developed. Ag-Pd@rGO is a highly active catalyst for SMCC and SCC reactions because the whole synthesis process needs no dispersants. Meanwhile, these catalytic reactions employ mild, efficient, ligand-free and heterogeneous conditions. More interestingly, oxygen can be used as the **"switch"** to control products in the SCC reaction. This simple, straightforward and general method is useful for the facile preparation of supported metal nanocatalysts.

Acknowledge

Funding from the National Science Foundation of China (21202115, 21276181, and 21074089) is gratefully acknowledged.

References

[1] X. Chen, G. Wu, J. Chen, X. Chen, Z. Xie and X. Wang, *J. Am. Chem. Soc.* 2011, **133**, 3693–3695.

[2] M. B. Thathagar, J. E. Elshof and G. Rothenberg, *Angew. Chem. Int. Ed.* 2006, **45**, 2886–2890.

[3] K. K. Nanda, A. Maisels, F. E. Kruis, H. Fissan and S. Stappert, *Phys. Rev. Lett.* 2003, **91**, 106102–106105.

[4] A. C. Balazs, T. Emrick and T. P. Russell, *Science* 2006, **314**, 1107–1110.

[5] C. Huang, C. Li and S. Shi, *Energy Environ. Sci.* 2012, **5**, 8848–8868.

[6] N. Zhang, Y. Zhang and Y. J. Xu, *Nanoscale* 2012, **4**, 5792–5813.

View Article Online
DOI: 10.1039/C4RA05186F

[7] N. Zhang, H. Qiu, Y. Liu, W. Wang, Y. Li, X. Wang and J. Gao, *J. Mater. Chem.* 2011, **21**, 11080–11083.

[8] Q. Zeng, J. Cheng, L. Tang, X. Liu, Y. Liu, J. Li and J. Jiang, *Adv. Funct. Mater.* 2010, **20**, 3366–3372.

[9] S. Stankovich, D. A. Dikin, G. H. B. Dommett, K. M. Kohlhaas, E. J. Zimney, E. A. Stach, R. D. Piner, S. T. Nguyen and R. S. Ruoff, *Nature* 2006, **442**, 282–286.

[10] M. J. Allen, V. C. Tung and R. B. Kaner, *Chem. Rev.* 2010, **110**, 132–145.

[11] C. Tan, X. Huang and H. Zhang, *Mater. Today* 2013, **16**, 29–36.

[12] G. M.Scheuermann, L. Rumi, P. Steurer, W. Bannwarth, R. Mülhaupt, *J. Am. Chem. Soc.* 2009, **131**, 8262–8270.

[13] D. R. Dreyer, S. Park, C. W. Bielawski and R. S. Ruoff, *Chem. Soc. Rev.* 2010, **39**, 228–240.

[14] Y. Guo, X. Sun, Y. Liu, W. Wang, H. Qiu and J. Gao, *Carbon* 2012, **50**, 2513–2523.

[15] M. Chen, L. Shen, S. Chen, H. Wang, X. Chen and J. Wang, *J. Mater. Chem. B* 2013, **1**, 2582–2589.

[16] F. Li, J. Song, H. Yang, S. Gan, Q. Zhang, D. Han, A. Ivaska and L. Niu, *Nanotechnology* 2009, **20**, 455602–455607.

[17] Y. Liang, H. Wang, H. S. Casalongue, Z. Chen and H. Dai, *Nano Research* 2010, **3**, 701–705.

[18] G. Yu, L. Hu, N. Liu, H. Wang, M. Vosgueritchian, Y. Yang, Y. Cui and Z. Bao, *Nano Lett.* 2011, **11**, 4438–4442.

[19] G. M. Scheuermann, L. Rumi, P. Steurer, W. Bannwarth and R. Mülhaupt, *J. Am. Chem. Soc.* 2009, **131**, 8262–8270.

View Article Online
DOI: 10.1039/C4RA05186F

[20] A. Molnár, *Chem. Rev.* 2011, **111**, 2251–2320.

[21] N. Miyaura and A. Suzuki, *Chem. Rev.* 1995, **95**, 2457–2483.

[22] D. Astruc, *Inorg. Chem.* 2007, **46**, 1884–1894.

[23] N. T. S. Phan, M. V. D. Sluys and C. W. Jones, *Adv. Synth. Catal.* 2006, **348**, 609–679.

[24] X. Jie, Y. Shang, P. Hu and W. Su, *Angew. Chem. Int. Ed.* 2013, **52**, 3630–3633.

[25] G. R. Desiraju, *Acc. Chem. Res.* 2002, **35**, 565–573.

[26] J. Ma, X. Wang, Y. Liu, T. Wu, Y. Liu, Y. Guo, R. Li, X. Sun, F. Wu, C. Li and J. Gao, *J. Mater. Chem. A* 2013, **1**, 2192–2201.

[27] S. Pei and H. Cheng, *Carbon* 2012, **50**, 3210–3228.

[28] D. Chen, L. Li and L. Guo, *Nanotechnology* 2011, **22**, 325601–325607.

[29] X. Zhou, J. Zhang, H. Wu, H. Yang, J. Zhang and S. Guo, *J. Phys. Chem. C* 2011, **115**, 11957–11961.

[30] H. J. Shin, K. K. Kim, A. Benayad, S. M. Yoon, H. K. Park, I. S. Jung, M. H. Jin, H. K. Jeong, J. M. Kim, J.Y. Choi and Y. H. Lee, *Adv. Funct. Mater.* 2009, **19**, 1987–1992.

[31] C. Amatore, A. Jutand and G. Le Duc, *Chem. Eur. J.* 2012, **18**, 6616–6625.

[32] J. Kim, L. J. Cote, F. Kim, W. Yuan, K. R. Shull and J. Huang, *J. Am. Chem. Soc.* 2010, **132**, 8180–8186.

[33] J. Li, Y. Liang and Y. Xie, *J. Org. Chem.* 2005, **70**, 4393–4396.